



# Visible light biophotosensors using biliverdin from *Antheraea yamamai*

JUNG WOO LEEM,<sup>1</sup> ANDRES E. LLACSAHUANGA ALLCCA,<sup>2</sup> JUNJIE CHEN,<sup>1</sup> SEONG-WAN KIM,<sup>3</sup> KEE-YOUNG KIM,<sup>3</sup> KWANG-HO CHOI,<sup>3</sup> YONG P. CHEN,<sup>2,5,6</sup> SEONG-RYUL KIM,<sup>3,4</sup> AND YOUNG L. KIM<sup>1,5,7,8,\*</sup>

<sup>1</sup>Weldon School of Biomedical Engineering, Purdue University, West Lafayette, IN 47907, USA

<sup>2</sup>Department of Physics and Astronomy, Purdue University, West Lafayette, IN 47907, USA

<sup>3</sup>Department of Agricultural Biology, National Institute of Agricultural Sciences, Rural Development Administration, Wanju, Jeollabuk-do 55365, South Korea

<sup>4</sup>ksr319@korea.kr

<sup>5</sup>Purdue Quantum Center, Purdue University, West Lafayette, IN 47907, USA

<sup>6</sup>Birck Nanotechnology Center, Purdue University, West Lafayette, IN 47907, USA

<sup>7</sup>Regenstrief Center for Healthcare Engineering, Purdue University, West Lafayette, IN 47907, USA

<sup>8</sup>Purdue Center for Cancer Research, Purdue University, West Lafayette, IN 47907, USA

\*youngkim@purdue.edu

**Abstract:** We report an endogenous photoelectric biomolecule and demonstrate that such a biomolecule can be used to detect visible light. We identify the green pigment abundantly present in natural silk cocoons of *Antheraea yamamai* (Japanese oak silkworm) as biliverdin, using mass spectroscopy and optical spectroscopy. Biliverdin extracted from the green silk cocoons generates photocurrent upon light illumination with distinct colors. We further characterize the basic performance, responsiveness, and stability of the biliverdin-based biophotosensors at a photovoltaic device level using blue, green, orange, and red light illumination. Biliverdin could potentially serve as an optoelectric biomolecule toward the development of next-generation implantable photosensors and artificial photoreceptors.

© 2018 Optical Society of America under the terms of the [OSA Open Access Publishing Agreement](#)

## 1. Introduction

Biliverdin, which is a biological green pigment, is known as a degradative intermediate associated with red blood cells and hemoglobin. It is formed by ring cleavage of heme catalyzed by the enzyme heme oxygenase [1,2]. Biliverdin can be found in a variety of green colored animals and insects (e.g. lizards, garfish, eggshells of birds, spiders, and silkworms) [3–9]. Biliverdin is also produced by microbes and plants [1,10,11]; biliverdin serves primarily as a precursor to photosensitive linear tetrapyrroles (e.g., phycocyanobilin and phycoerythrobilin) in cyanobacteria, red algae, and plants [12]. Biliverdin plays a role in cyanobacterial and algal light-harvesting phycobiliprotein complexes and light-sensing receptors (e.g. phytochrome) [13,14]. Importantly, as a chromophore as well as an antioxidant/anti-inflammation molecule, biliverdin has been used in a few bioimaging and therapeutic applications [15–19]. Although this natural nontoxic green pigment is abundant in nature, biliverdin has not yet been investigated as a photoelectric conversion biomaterial.

One of the sources to obtain a decent amount of biliverdin is silkworms and silk cocoons, in particular *Antheraea yamamai* (Japanese oak silkworm). Specifically, *Antheraea yamamai* has been cultivated for centuries as a native in East Asia [20,21]. Mimicking the natural sunlight exposure, when light with high intensity (5000 lux) is irradiated onto Japanese oak silkworms, the silk cocoon is colorized to be green due to the photochemical transformation to biliverdin [8,9]. In other words, biliverdin is also present in the silk cocoons of *Antheraea yamamai* [8,9]. As biliverdin absorbs the visible light in the broad wavelength range of mainly blue and red [22], the green color of the silk cocoon may provide a camouflage effect

in nature. Given that silkworms have been considered as bioreactors for producing recombinant proteins, the silk cocoons of *Antheraea yamamai* can be a source for mass-producing biliverdin. It should also be noted that silk cocoons and processed silk polymers are actively used for biomedical and optical applications, owing to the biocompatibility/biodegradation [23–25] and the superior mechanical and optical properties [26–28].

Although there are recent advances in implantable photosensors, these still rely on biocompatible, yet exogenous, materials (e.g., MoS<sub>2</sub>, graphene, Al<sub>2</sub>O<sub>3</sub>, Si<sub>3</sub>N<sub>4</sub>, and polyimide) [29]. In our study, we investigate whether there is any endogenous biomaterial that can be used for biological photosensors. Interestingly, animals, including of *Antheraea yamamai* and humans, can endogenously generate and metabolize biliverdin [4,30]. This means that biliverdin-based photosensors can be more biologically friendly to the human body and be useful for potentially developing next-generation implantable photosensors and artificial photoreceptors.

In this study, we introduce the photoelectric conversion property of biliverdin at a device level as a biophotosensor for detecting visible light. First, after harvesting *Antheraea yamamai* silk cocoons, we describe a processing method to extract biliverdin from the silk cocoons. Second, we fabricate prototype devices of the biophotosensors. Third, we conduct comprehensive physical and chemical analyses, including mass spectrometry, optical measurements, and photoluminescence (PL) measurements. Finally, we demonstrate the basic current-voltage characteristics and stability of the biophotosensors under visible light illumination with distinct colors. We envision that the reported photovoltaic characteristics of biliverdin could potentially be used for biological and medical applications.

## 2. Experiments and methods

### 2.1 Production, materials, and chemicals

We harvested silk cocoons produced by *Antheraea yamamai* in the experimental farm of the National Institute of Agricultural Sciences in the Republic of Korea. *Antheraea yamamai* silkworms were reared in an outdoor-breeding farm planted with oak trees, as shown in Fig. 1(a). To protect the hatched larvae from damage caused by birds and rats, the farm was covered with a net. The eggs of *Antheraea yamamai* were released to oak trees. After completion of cocoon spinning, the green cocoons were collected and then the silkworm pupae were removed. The silk cocoon of *Antheraea yamamai*, which was reared in the outdoor sunlight environment, exhibits a green color due to its strong reflectance in the wavelength range of 490 – 590 nm, as shown in Fig. 1(b). The rearing time for a growth period of *Antheraea yamamai* is summarized in Table 1.

To extract biliverdin and construct prototypes of biliverdin-based biophotosensors, we used the following chemicals and materials. Titanium dioxide (TiO<sub>2</sub>) paste with particle sizes of 15 – 20 nm (Ti-Nanoxide T/SP, anatase phase) and fluorine-doped tin oxide (FTO)-coated conducting glasses (sheet resistance 7 Ω sq<sup>-1</sup>, transmittance > 70% in the wavelengths of 470 – 1100 nm) were purchased from SOLARONIX S.A. (Aubonne, Switzerland). Sodium carbonate (Na<sub>2</sub>CO<sub>3</sub>, ≥ 99.5%), Miracloth (pore sizes of 22 – 25 μm), dimethyl sulfoxide (DMSO; (CH<sub>3</sub>)<sub>2</sub>SO, 99%), titanium(IV) chloride (TiCl<sub>4</sub>) solution (0.09 M in 20% HCl), EL-HPE (High Performance Electrolyte, Dyesol), Sylgard 184 (Dow Corning Co.), and Parafilm were purchased from Sigma-Aldrich Co. (Milwaukee, WI, USA). Deionized water (Milli-Q system) was used. All chemicals were used without further purification. The experiments were performed under the ambient conditions (22 ± 2 °C and 40 ± 10% relative humidity).

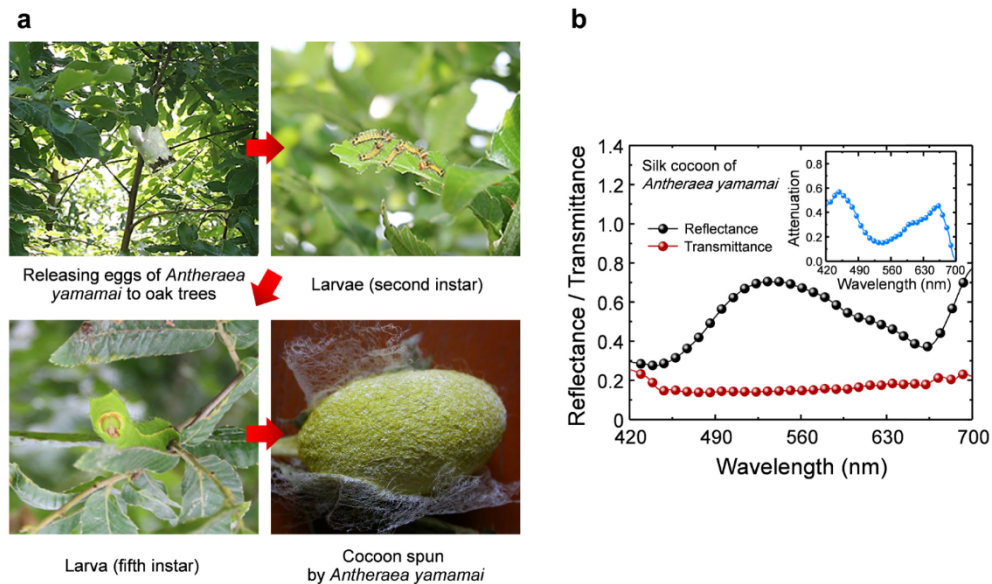


Fig. 1. (a) Photographs of growth periods for *Antheraea yamamai* silkworms rearing in an outdoor-breeding farm planted with oak trees (National Institute of Agricultural Sciences, Republic of Korea). (b) Optical properties of the degummed silk cocoon of *Antheraea yamamai* measured using an integrating sphere (Attenuation = 1 – Transmittance – Reflectance).

Table 1. Rearing time for a growth period of *Antheraea yamamai*

Growth period	Rearing time (day)
First instar	6
Second instar	11
Third instar	5
Fourth instar	9
Fifth instar	14

## 2.2 Extraction of biliverdin from *Antheraea yamamai* silk cocoons

To facilitate the extraction of biliverdin, we first removed sericin in the silk cocoons using a chemical and physical degumming method via a low-temperature process for minimizing the heat-induced denaturation of biliverdin. The silk cocoons were soaked into a degumming solution ( $\text{Na}_2\text{CO}_3$ ,  $2.5 \text{ g l}^{-1}$ ) with stirring of 400 rpm at  $60^\circ\text{C}$  for three hours and then were washed with warmed deionized water. The degumming process was repeated three times. The resultant degummed silk cocoons were dried at room temperature under a dark condition.

We developed a simple protocol to extract biliverdin from the degummed silk cocoons using dimethyl sulfoxide (DMSO) as a solvent (Fig. 2). DMSO has relatively low toxicity and is an environmentally benign organic solvent [31]. After the degumming process, the silk cocoons were cut into small pieces with sizes of  $< 10 \text{ mm}$  and then were immersed in the DMSO solvent with a concentration of  $0.1 \text{ g ml}^{-1}$  with stirring of 400 rpm at  $45^\circ\text{C}$  for 24 hours. Then, the DMSO solvent effectively released biliverdin from the silk cocoons. After removing the cocoon pieces, the green residual solution was centrifuged with 9000 rpm for 20 minutes at room temperature. The final solution was stored at room temperature in dark before use.

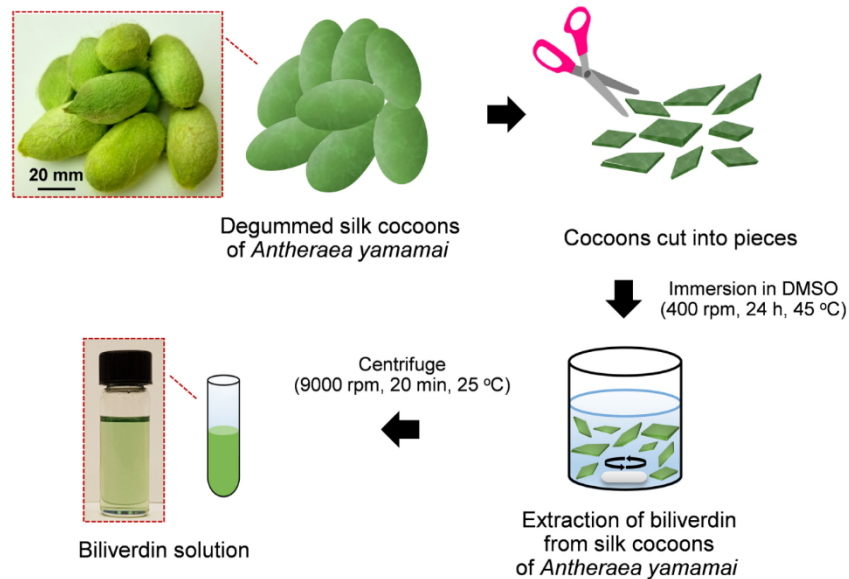


Fig. 2. Schematic diagram for an extraction process of biliverdin from the green cocoons of *Antheraea yamamai*. The photographs are the degummed green cocoons of *Antheraea yamamai* and the extracted biliverdin solution.

### 2.3 Device fabrication of biliverdin-based biophotosensor prototypes

As the first testing device using a biliverdin solution, we constructed working prototypes of the biliverdin-based biophotosensors. Specifically, we mimicked the simple device structure of typical dye-sensitized solar cells, as commonly used elsewhere [32,33]. First, a photoanode electrode was prepared on the conducting side of FTO glass substrate by coating a commercial transparent  $\text{TiO}_2$  paste. The uniform coating thickness of 10  $\mu\text{m}$  was achieved using a doctor-blade (tape casting) method. Before coating, the substrate was cleaned in an ultrasonic bath using acetone, methanol, and deionized water, followed by blowing with nitrogen gas. To remove organic components in the coated  $\text{TiO}_2$  paste, the substrate was subsequently annealed at 120 °C for 15 minutes, at 350 °C for 15 minutes, and at 475 °C for 30 minutes on a hot plate, followed by naturally cooling down to 100 °C. To ensure the physical contact among  $\text{TiO}_2$  nanoparticles, the  $\text{TiO}_2$  photoanode was additionally immersed into an aqueous solution of 15 mM  $\text{TiCl}_4$  at 70 °C for 30 minutes in an oven. Second, a biliverdin solution (10  $\mu\text{l}$ ) extracted from the silk cocoons was dropped on the  $\text{TiO}_2$ -coated photoanode. The volume of the biliverdin solution was controlled by a punched polydimethylsiloxane (PDMS) template with a diameter of 6 mm, which prevented the solution from diffusion. The sample was dried at 40 °C for above six hours in an oven. Third, an anode electrode was assembled with a platinum (Pt)-coated FTO glass substrate as a counter electrode in a sandwich geometry by a hot-melt Parafilm. For good electrical contact, the external electrodes were coated with a silver paste. Finally, an electrolyte solution was injected into a space created by the Parafilm through pre-drilled channel holes on the counter electrode, followed by sealing with the Parafilm and a thin glass cover. For devices without using an electrolyte, the original biliverdin solution was also directly tested by injecting it into the assembled structure.

### 2.4 Mass spectrometry analysis

We obtained positive ion spectra using a mass spectrometer (6550 iFunnel Q-TOF, Agilent Technologies, Santa Clara, CA, USA). A biliverdin solution (3  $\mu\text{l}$ ) extracted from the silk cocoons was injected into a Zorbax Extend  $\text{C}_{18}$  column. The two components of the mobile

phase (A and B) were used such that A was 0.1% formic acid in water and B was methanol. The gradient was 10% B for one minute, 55% B for two minutes, and 90% B for four minutes, respectively. The flow was  $0.2 \text{ ml min}^{-1}$ . Selected reaction monitoring (SRM) spectra were obtained with  $583[\text{M} + \text{H}]^+$  transitioning to  $m/z$  297.

## 2.5 Optical characterizations

We characterized the optical properties including reflectance, transmittance, absorption, and PL spectra/images using a fiber bundle-coupled spectrometer with an integrating sphere and a customized mesoscopic spectrometer setup, as reported in our previous studies [24,34]. In particular, PL analysis was highly useful to better understand the charge carrier trapping, migration, and recombination processes between photosensitizing molecules and metal oxide materials, because PL emission originates from the recombination of free carriers in the molecules [35–37]. A customized template for containing the biliverdin solution was prepared as shown in Fig. 3(a). A  $\text{TiO}_2$  film with a diameter of 4 mm was coated on the cleaned glass microscope slide using the doctor-blade method and was subsequently cured at different temperatures of  $120 \text{ }^\circ\text{C}$  (15 minutes),  $350 \text{ }^\circ\text{C}$  (15 minutes), and  $475 \text{ }^\circ\text{C}$  (30 minutes), respectively. A 1 mm-thick PDMS template was made from Sylgard 184 silicone elastomers kit with a ratio of 10:1 (base:agent). After curing, the PDMS template was punched with a diameter of 10 mm and then was laminated on the  $\text{TiO}_2$ -coated glass. A biliverdin solution ( $50 \mu\text{l}$ ) in DMSO was dropped on the  $\text{TiO}_2$ -coated glass area in the PDMS template. To detect PL emission of biliverdin, the fabricated template was placed within the field of view of the mesoscopic imaging setup, in which an excitation source at  $\lambda_{\text{ex}} = 470 \text{ nm}$  and an emission filter with  $\lambda_{\text{em}} = 600 - 800 \text{ nm}$  were used, as shown in Fig. 3(b).

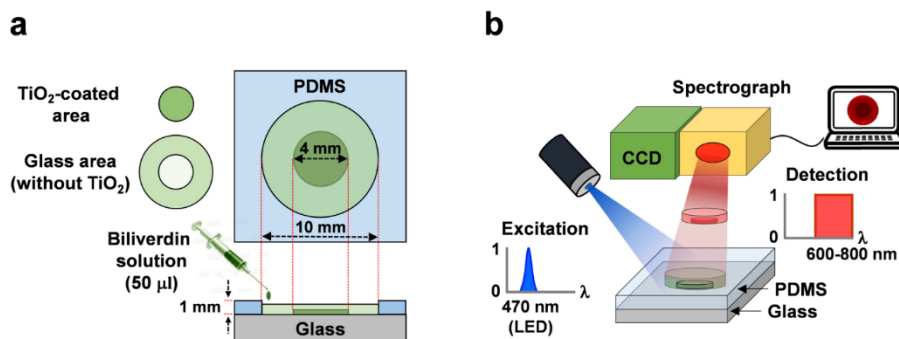


Fig. 3. Schematic illustrations for the specimen template (a) and the imaging measurement configuration (b). A biliverdin solution is dropped onto the punched PDMS template. The PL emission is detected via an emission filter ( $\lambda_{\text{em}} = 600 - 800 \text{ nm}$ ) when illuminated with an excitation source ( $\lambda_{\text{ex}} = 470 \text{ nm}$ ).

## 2.6 Current density-voltage response analyses

We measured the current density–voltage ( $J$ – $V$ ) characteristics of the biophotosensors using a source meter (2400, Keithley Instruments Inc., Cleveland, OH, USA) controlled by a customized LabView interface. For time-resolved photocurrent measurements, a low-noise current preamplifier (SR570, Stanford Research Systems) and a real-time digital oscilloscope (DPO7104, 10 GS/s, 1 GHz, Tektronix) were employed. As visible light sources, blue, green, orange, and red LEDs (Thorlabs Inc., Newton, NJ, USA) were used with different center wavelengths of 470 nm (FWHM = 25 nm), 530 nm (FWHM = 33 nm), 565 nm (FWHM = 104 nm), and 625 nm (FWHM = 18 nm), respectively. The LED power was tuned by controlling the LED drive current (LEDD1B, Thorlabs Inc.) and was calibrated using a power meter (PM100D, Thorlabs Inc.). Importantly, a black mask with a diameter of 6 mm was

utilized to ensure accurate measurements of the incident light. All of the measurements were carried out in a dark and shielded enclosure at room temperature.

### 3. Results and discussion

First, we confirmed that biliverdin is the dominant molecule in the green solution extracted from the silk cocoons of *Antheraea yamamai*, using the mass spectral analysis. As shown in the mass spectrum (Fig. 4(a)), the main peak at  $m/z$  583.2877 corresponds to the molecular ion of biliverdin (exact mass 583.2557 Da, protonated form) [38,39]. The light absorption spectrum also shows the green color; the strong light absorption is observed at around blue (maximum  $\lambda_{\text{abs}} = 445$  nm) and red (maximum  $\lambda_{\text{abs}} = 603$  nm) wavelength ranges, while its weak absorption is shown in the green wavelength (minimum  $\lambda_{\text{abs}} = 515$  nm) in Fig. 4(b). Importantly, biliverdin is a fluorescent biomolecule; it emits red fluorescent light with a maximum emission wavelength ( $\lambda_{\text{em}}$ ) of 674 nm when excited at 450 nm, as shown in Fig. 4(c). Indeed, all of the optical properties of the extracted green solution are in good agreement with the previous studies about biliverdin [22,40].

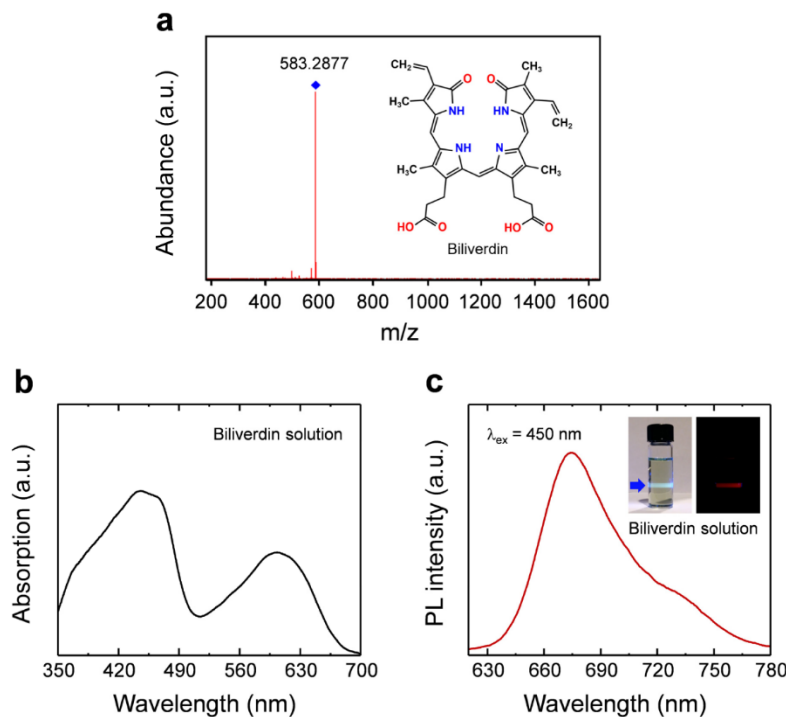


Fig. 4. (a) Mass spectrum of the green pigment extracted from the silk cocoons of *Antheraea yamamai*. The distinct peak at  $m/z$  583.2877 is in good agreement with the molecular ion of biliverdin (exact mass 583.2557 Da, protonated form) (Refs. [38,39]). Structure of biliverdin is shown in the inset of (a). Optical absorption (b) and photoluminescence (PL) (c) spectra of the biliverdin solution. Photographs of the biliverdin solution and its fluorescence emission excited at  $\lambda_{\text{ex}} = 450$  nm are shown in the inset of (c).

Second, we studied photoinduced electron transfer between biliverdin (donor) to  $\text{TiO}_2$  (acceptor) on the basis of the PL emission of biliverdin. Figure 5 depicts the PL image of biliverdin on the  $\text{TiO}_2$ -coated glass surrounded by the PDMS template and the cross-sectional spatial profile along A to B (white dashed line). The PL intensity of biliverdin on the  $\text{TiO}_2$ -coated area is lower than that of the glass area without  $\text{TiO}_2$ . The percentage decrease in the PL intensity is approximately 15%. This reduction was attributed to the quenching of biliverdin molecules, which were adsorbed to  $\text{TiO}_2$  nanoparticles (i.e. physical contact

between biliverdin and TiO<sub>2</sub> nanoparticles), strongly suggesting photoinduced electron transfer from biliverdin into TiO<sub>2</sub> [35]. This result supports the idea that biliverdin can act as a photoelectric biomolecule.

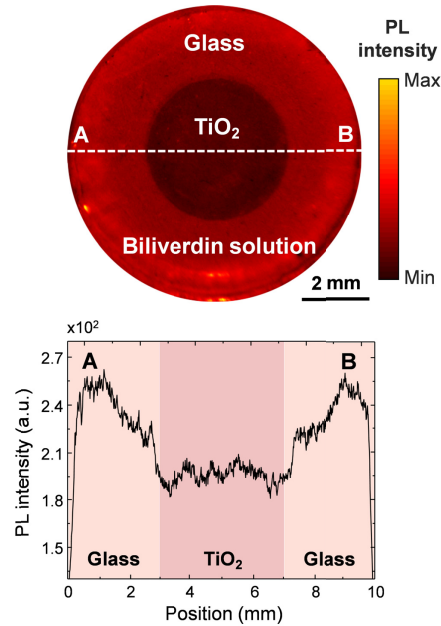


Fig. 5. Quenching of biliverdin emission possibly due to electron transfer to TiO<sub>2</sub>. The PL intensity image of the biliverdin solution on the TiO<sub>2</sub>-coated glass surrounded by the PDMS template (upper) at  $\lambda_{\text{ex}} = 470$  nm and the cross-sectional spatial profile along A to B (white dashed line in the PL intensity image).

Third, we tested the device performance of biliverdin-based biophotosensors constructed without using an electrolyte as shown in Fig. 6(a). Without using an electrolyte, the biliverdin solution in DMSO was directly injected into a space between both of the electrodes created by the Parafilm through pre-drilled channel holes on the counter electrode. Under blue light illumination ( $\lambda = 470$  nm and  $15 \text{ mW cm}^{-2}$ ), the photocurrent (short-circuit current density  $J_{\text{sc}}$ ) of  $0.884 \mu\text{A cm}^{-2}$  at zero bias was obtained, resulting in a light on/off ratio ( $J_{\text{light}}/J_{\text{dark}}$ ) of  $\sim 100$ . Importantly, despite the absence of an electrolyte, the photocurrent was generated. It is highly likely that this was attributed to the presence of ionic elements in our biliverdin solution, such as calcium (Ca), sodium (Na), chlorine (Cl), magnesium (Mg), and potassium (K). It is well known that natural silk cocoons contain some amount of these trace elements, which could allow the silk fibers to be a conducting medium in water or high-humidity environments [41–43]. Thus, we checked if other chemical constituents of the extracted biliverdin solution can contribute to the photoresponsivity. For comparison with *Antheraea yamamai* silk, white silk cocoons of *Bombyx mori* (Baekokjam) were used as a control. Using the same fabrication process of the biliverdin solution, we obtained a solution from white silk. This solution was directly injected into the assembled device without using an electrolyte. Under blue light illumination ( $\lambda = 470$  nm and  $15 \text{ mW cm}^{-2}$ ), it did not generate any photocurrent. In other words, other chemical constituents, such as ionic elements, are not responsible for photocurrent generation under visible light illumination.

To effectively collect the photoinduced charge carriers, we further used a commercial high-performance electrolyte. Figure 6(b) shows the  $J$ - $V$  characteristics under blue light illumination ( $\lambda = 470$  nm) with the light intensity of  $15 \text{ mW cm}^{-2}$ . At zero bias (i.e. 0 V) in the self-power mode without applying external power to the device, an on/off ratio of  $J_{\text{sc}}$

signals was evaluated as high as  $\sim 2.53 \times 10^3$  (i.e.  $J_{\text{dark}} = 0.003 \mu\text{A cm}^{-2}$  and  $J_{\text{light}} = 7.579 \mu\text{A cm}^{-2}$ ). The photoresponsivity  $R = J_{\text{photo}}/P_{\text{light}}$  was also calculated to be  $\sim 0.505 \text{ mA W}^{-1}$ , where the photocurrent density  $J_{\text{photo}}$  is determined by  $J_{\text{light}} - J_{\text{dark}}$  and  $P_{\text{light}}$  is the incident light intensity (i.e.  $15 \text{ mW cm}^{-2}$ ). As another key property for photosensors, the relationship between the photogenerated current and voltage and the intensity of the incident light was further studied under the blue light illumination ( $\lambda = 470 \text{ nm}$ ) in Fig. 6(c).  $J_{\text{sc}}$  increases linearly from 2.217 to  $23.868 \mu\text{A cm}^{-2}$  as a function of the light intensity in a variation range from 5 to  $45 \text{ mW cm}^{-2}$ . On the other hand, the increase in the open-circuit voltage ( $V_{\text{oc}}$ ) follows nonlinear dependence on the light intensity due to the proportional relationship of  $V_{\text{oc}}$  and  $\ln(J_{\text{light}}/J_{\text{dark}})$ .

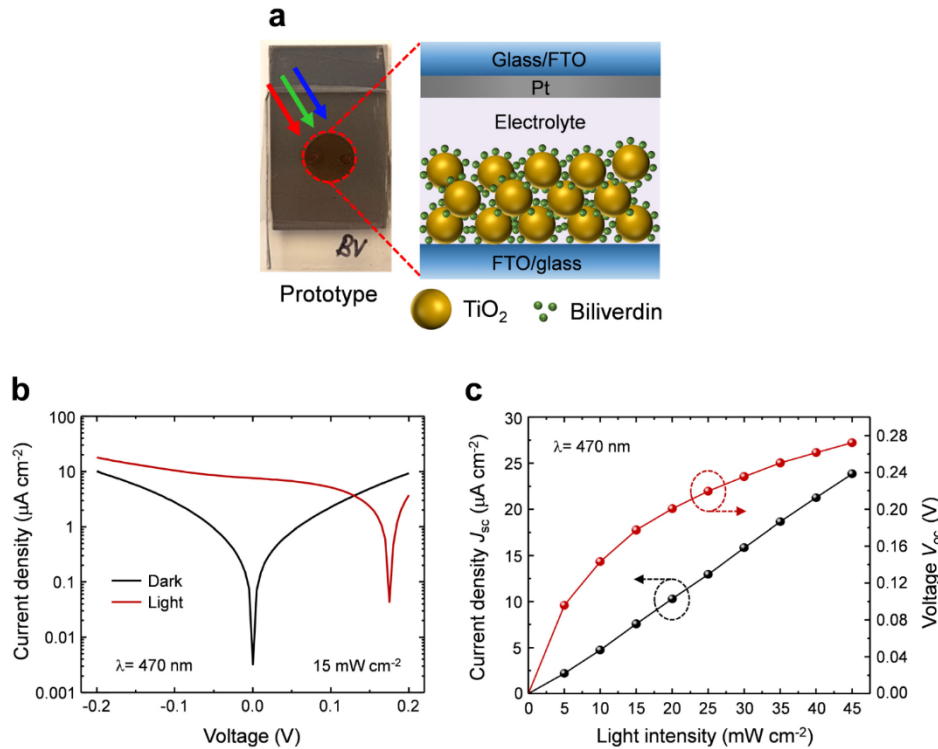


Fig. 6. Current density-voltage ( $J$ - $V$ ) response analysis of the biliverdin-based biophotosensors. (a) Photograph of our photosensor device prototype (left) and the schematic illustration of the corresponding device structure (right). (b)  $J$ - $V$  characteristics of the biophotosensors in the light-on and -off states. (c) Short-circuit current density ( $J_{\text{sc}}$ ) and open-circuit voltage ( $V_{\text{oc}}$ ) as a function of the light intensity under blue illumination ( $\lambda = 470 \text{ nm}$ ).

Next, we tested the responsiveness of the biliverdin-based biophotosensors. Specifically, we quantified switching behavior of  $J_{\text{sc}}$  and  $V_{\text{oc}}$  in the light-on and -off states upon visible light illumination in different central wavelengths of 470 nm, 530 nm, 565 nm, and 625 nm at  $15 \text{ mW cm}^{-2}$ , as shown in Fig. 7(a) and 7(b). Both  $J_{\text{sc}}$  and  $V_{\text{oc}}$  were reproducibly switched from the 'high' state to the 'low' state by periodically turning each light source on and off. As expected, the dependence of  $J_{\text{sc}}$  and  $V_{\text{oc}}$  on the incident wavelength reflected the absorption spectrum of biliverdin in Fig. 4(b). The light on/off ratios of the biophotosensors for  $J_{\text{sc}}$  were estimated to be  $\sim 310$ ,  $\sim 595$ , and  $\sim 39$  at 530 nm, 565 nm, and 625 nm, respectively.

We also characterized the response speed of the biophotosensors by calculating the rise time  $R_t$  and the decay time  $D_t$ .  $R_t$  was defined as a time interval to rise from 10% to 90% of its peak value, while  $D_t$  was defined as a time interval to decay from 90% to 10% of its peak

value. As shown in the current and voltage responses in Fig. 7(c) and 7(d),  $R_t$  and  $D_t$  values of the biophotosensors are  $\sim 0.09$  and  $\sim 0.08$  second for  $J_{sc}$  and  $\sim 0.305$  and  $\sim 1.134$  second for  $V_{oc}$ , respectively. For  $J_{sc}$ , the biliverdin biophotosensors show the relatively rapid photoresponse characteristics. On the contrary, for  $V_{oc}$ , the biophotosensors exhibit the slow photoresponse with much longer  $R_t$  and  $D_t$ . This behavior can be understood by a slow recombination rate of photogenerated electrons by electrolyte ions on the  $\text{TiO}_2$ /electrolyte interface, because there was no current passing through the external circuit under the  $V_{oc}$  condition [44].

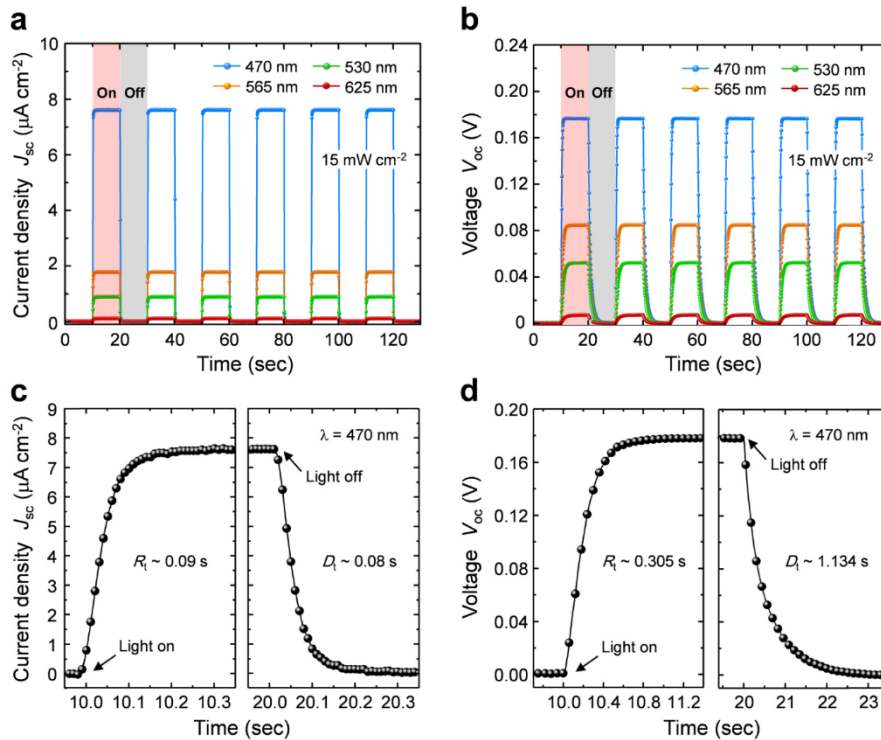


Fig. 7. Time responses of  $J_{sc}$  (a) and  $V_{oc}$  (b) measured for the light-on and -off states upon light illuminations in several different visible wavelengths of 470, 530, 565, and 625 nm ( $15 \text{ mW cm}^{-2}$ ). Rising and decaying edges are zoomed to estimate the rise time  $R_t$  and the decay time  $D_t$  for  $J_{sc}$  (c) and  $V_{oc}$  (d) at  $\lambda = 470 \text{ nm}$  ( $15 \text{ mW cm}^{-2}$ ).

Finally, given that all fluorescent molecules are subject to photobleaching [45,46], we determined the stability of the biophotosensors. We characterized real-time photocurrent ( $J_{sc}$ ) transient responses by periodically switching an optical signal on and off at 0.5 Hz under the blue light illumination ( $\lambda = 470 \text{ nm}$ ,  $15 \text{ mW cm}^{-2}$ ). Figure 8(a) shows that the biophotosensor is switched between the light on- and off-states with relatively good reproducibility and stability. After photoswitching cycles of 2000, the photocurrent was reached to be  $6.828 \mu\text{A cm}^{-2}$ , but the percentage decrease was only 10% compared to its initial value (i.e.  $J_{sc} = 7.579 \mu\text{A cm}^{-2}$ ). In addition, to check the practicality of the biliverdin-based biophotosensors, we determined the long-term stability for an extended period of 1440 hours (60 days) in Fig. 8(b). The biophotosensors were stored in the lab under the ambient conditions ( $22 \pm 2 \text{ }^\circ\text{C}$  and 40 – 50% relative humidity). After 1440 hours, the photocurrent was highly retained with a percent decrease of  $\sim 8\%$  ( $J_{sc} = 6.981 \mu\text{A cm}^{-2}$ ). The decrease in  $J_{sc}$  is attributable mainly to the photobleaching of biliverdin by light excitation. In addition, other deteriorating factors at the device level over time can include reduction in the triiodide ( $\text{I}_3^-$ ) concentration in the acetonitrile-based iodide/triiodide ( $\text{I}^-/\text{I}_3^-$ ) electrolyte and degradation of the anode and counter

electrodes [45–47]. However, this result supports that idea that biliverdin can be stable even when contacted with  $\text{TiO}_2$  and the electrolyte.

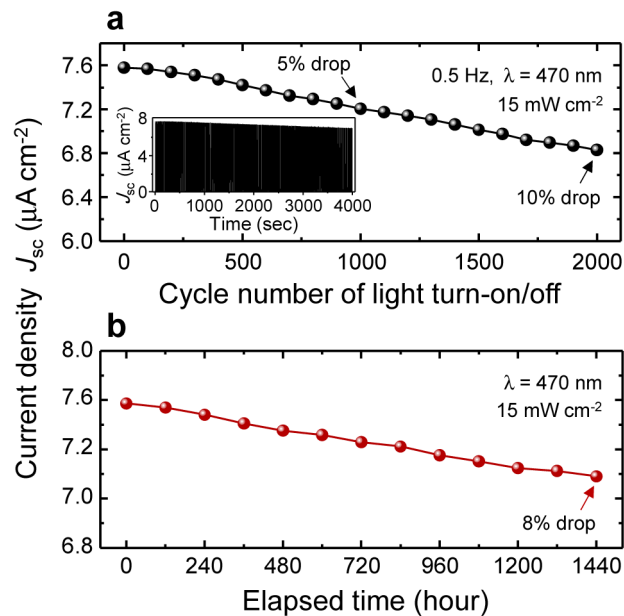


Fig. 8. Device stability of the biliverdin-based biophotosensors. (a) Cyclic response on  $J_{sc}$  in the light-on and -off states upon light illumination ( $0.5 \text{ Hz}$ ,  $\lambda = 470 \text{ nm}$ ,  $15 \text{ mW cm}^{-2}$ ) as a function of an on/off cycle number. The inset shows the time response of  $J_{sc}$ . (b) Long-term stability when the photosensors were placed in the laboratory under the ambient conditions ( $22 \pm 2 \text{ }^\circ\text{C}$  and 40 – 50% relative humidity).

#### 4. Conclusion

We have demonstrated the photovoltaics of biliverdin extracted from the silk cocoons of *Antheraea yamamai* in the photosensor prototypes. Although biliverdin has been used in bioimaging, the photoelectric conversion of biliverdin has not yet been used at a device level to the best of our knowledge. Mass spectroscopy and optical spectroscopy confirm that the silk cocoons of *Antheraea yamamai* contains biliverdin. Fluorescent quenching of biliverdin in the presence of  $\text{TiO}_2$  in the PL analysis supports possible photoinduced electron transfer. In the self-power mode (i.e. zero bias), the biliverdin-based biophotosensors are successfully operated under visible light illumination at 470 nm, 530 nm, 565 nm, and 625 nm. The reliable responsiveness is tested from repeated on/off switching. In addition, this environmental-friendly production and biocompatible nature of biliverdin could potentially provide with a simple and cost-effective manufacturing strategy.

#### Funding

Agenda Program (PJ01270901) in Rural Development Administration, South Korea; Cooperative Research Program for Agriculture Science & Technology Development (PJ012089) in Rural Development Administration, South Korea; Air Force Office of Scientific Research (FA2386-17-1-4072) in the USA; and Discovery Park Big Idea Challenge from Purdue University in the USA.

#### Disclosures

The authors declare that there are no conflicts of interest related to this article.

## References

1. D. Chen, J. D. Brown, Y. Kawasaki, J. Bommer, and J. Y. Takemoto, "Scalable production of biliverdin IX $\alpha$  by *Escherichia coli*," *BMC Biotechnol.* **12**(1), 89 (2012).
2. T. W. Sedlak and S. H. Snyder, "Bilirubin benefits: Cellular protection by a biliverdin reductase antioxidant cycle," *Pediatrics* **113**(6), 1776–1782 (2004).
3. C. C. Austin and K. W. Jessing, "Green-blood pigmentation in lizards," *Comp. Biochem. Phys. A* **109**(3), 619–626 (1994).
4. Z. B. Rodriguez, S. L. Perkins, and C. C. Austin, "Multiple origins of green blood in New Guinea lizards," *Sci. Adv.* **4**, 5017 (2018).
5. F. Jüttner, M. Stiesch, and W. Ternes, "Biliverdin: the blue-green pigment in the bones of the garfish (*Belone belone*) and eelpout (*Zoarces viviparus*)," *Eur. Food Res. Technol.* **236**(6), 943–953 (2013).
6. R. Zhao, G. Y. Xu, Z. Z. Liu, J. Y. Li, and N. Yang, "A study on eggshell pigmentation: Biliverdin in blue-shelled chickens," *Poult. Sci.* **85**(3), 546–549 (2006).
7. A. Holl and W. Rüdiger, "Micromatabilin, a new biliverdin conjugate in the spider, *Micromata-rosea* (Sparassidae)," *J. Comp. Physiol.* **98**, 189–191 (1975).
8. Y. Kato, Y. Onuma, K. Sakurai, and H. Yamada, "Role of light in the green pigmentation of cocoons of *Antheraea yamamai* (Lepidoptera, Saturniidae)," *Appl. Entomol. Zool.* **24**(4), 398–406 (1989).
9. H. Yamada and Y. Kato, "Green colouration of cocoons in *Antheraea yamamai* (Lepidoptera: Saturniidae): light-induced production of blue bilin in the larval haemolymph," *J. Insect Physiol.* **50**(5), 393–401 (2004).
10. T. Muramoto, N. Tsurui, M. J. Terry, A. Yokota, and T. Kohchi, "Expression and biochemical properties of a ferredoxin-dependent heme oxygenase required for phytochrome chromophore synthesis," *Plant Physiol.* **130**(4), 1958–1966 (2002).
11. A. Wilks and M. P. Schmitt, "Expression and characterization of a heme oxygenase (Hmu O) from *Corynebacterium disphtheriae*. Iron acquisition requires oxidative cleavage of the heme macrocycle," *J. Biol. Chem.* **273**(2), 837–841 (1998).
12. W. M. Schluchter and A. N. Glazer, "Characterization of cyanobacterial biliverdin reductase. Conversion of biliverdin to bilirubin is important for normal phycobiliprotein biosynthesis," *J. Biol. Chem.* **272**(21), 13562–13569 (1997).
13. T. D. Elich, A. F. McDonagh, L. A. Palma, and J. C. Lagarias, "Phytochrome chromophore biosynthesis. Treatment of tetrapyrrole-deficient *Avena* explants with natural and non-natural bilatrienes leads to formation of spectrally active holoproteins," *J. Biol. Chem.* **264**(1), 183–189 (1989).
14. E. Giraud, J. Fardoux, N. Fourrier, L. Hannibal, B. Genty, P. Bouyer, B. Dreyfus, and A. Verméglio, "Bacteriophytochrome controls photosystem synthesis in anoxygenic bacteria," *Nature* **417**(6885), 202–205 (2002).
15. D. Yu, W. C. Gustafson, C. Han, C. Lafaye, M. Noirclerc-Savoie, W. P. Ge, D. A. Thayer, H. Huang, T. B. Kornberg, A. Royant, L. Y. Jan, Y. N. Jan, W. A. Weiss, and X. Shu, "An improved monomeric infrared fluorescent protein for neuronal and tumour brain imaging," *Nat. Commun.* **5**(1), 3626 (2014).
16. R. Narikawa, T. Nakajima, Y. Aono, K. Fushimi, G. Enomoto, S. Ni-Ni-Win, S. Itoh, M. Sato, and M. Ikeuchi, "A biliverdin-binding cyanobacteriochrome from the chlorophyll *d*-bearing cyanobacterium *Acaryochloris marina*," *Sci. Rep.* **5**(1), 7950 (2015).
17. X. Shu, A. Royant, M. Z. Lin, T. A. Aguilera, V. Lev-Ram, P. A. Steinbach, and R. Y. Tsien, "Mammalian expression of infrared fluorescent proteins engineered from a bacterial phytochrome," *Science* **324**(5928), 804–807 (2009).
18. G. S. Filonov, K. D. Piatkevich, L. M. Ting, J. Zhang, K. Kim, and V. V. Verkhusha, "Bright and stable near-infrared fluorescent protein for *in vivo* imaging," *Nat. Biotechnol.* **29**(8), 757–761 (2011).
19. R. Öllinger, H. Wang, K. Yamashita, B. Wegiel, M. Thomas, R. Margreiter, and F. H. Bach, "Therapeutic applications of bilirubin and biliverdin in transplantation," *Antioxid. Redox Signal.* **9**(12), 2175–2186 (2007).
20. S. R. Kim, M. I. Kim, M. Y. Hong, K. Y. Kim, P. D. Kang, J. S. Hwang, Y. S. Han, B. R. Jin, and I. Kim, "The complete mitogenome sequence of the Japanese oak silkworm, *Antheraea yamamai* (Lepidoptera: Saturniidae)," *Mol. Biol. Rep.* **36**(7), 1871–1880 (2009).
21. S. R. Kim, W. Kwak, H. Kim, K. Caetano-Anolles, K. Y. Kim, S. B. Kim, K. H. Choi, S. W. Kim, J. S. Hwang, M. Kim, I. Kim, T. W. Goo, and S. W. Park, "Genome sequence of the Japanese oak silk moth, *Antheraea yamamai*: the first draft genome in the family Saturniidae," *Gigascience* **7**(1), 1–11 (2018).
22. R. Shah, J. Schwach, N. Frankenberg-Dinkel, and W. Gärtner, "Complex formation between heme oxygenase and phytochrome during biosynthesis in *Pseudomonas syringae* pv. *tomato*," *Photochem. Photobiol. Sci.* **11**(6), 1026–1031 (2012).
23. K. Hu, Q. Lv, F. Z. Cui, Q. L. Feng, X. D. Kong, H. L. Wang, L. Y. Huang, and T. Li, "Biocompatible fibroin blended films with recombinant human-like collagen for hepatic tissue engineering," *J. Bioact. Compat. Polym.* **21**(1), 23–37 (2006).
24. J. W. Leem, J. Park, S. W. Kim, S. R. Kim, S. H. Choi, K. H. Choi, and Y. L. Kim, "Green-light-activated photoreaction via genetic hybridization of far-red fluorescent protein and silk," *Adv. Sci. (Weinh.)* **5**(6), 1700863 (2018).
25. R. L. Horan, K. Antle, A. L. Collette, Y. Wang, J. Huang, J. E. Moreau, V. Volloch, D. L. Kaplan, and G. H. Altman, "In vitro degradation of silk fibroin," *Biomaterials* **26**(17), 3385–3393 (2005).

26. K. Numata, R. Sato, K. Yazawa, T. Hikima, and H. Masunaga, "Crystal structure and physical properties of *Antheraea yamamai* silk fibers: Long poly(alanine) sequences are partially in the crystalline region," *Polymer (Guildf.)* **77**, 87–94 (2015).
27. J. W. Leem, S. H. Choi, S. R. Kim, S. W. Kim, K. H. Choi, and Y. L. Kim, "Scalable and continuous nanomaterial integration with transgenic fibers for enhanced photoluminescence," *Mater. Horiz.* **4**(2), 281–289 (2017).
28. S. H. Choi, S. W. Kim, Z. Ku, M. A. Visbal-Onufrak, S. R. Kim, K. H. Choi, H. Ko, W. Choi, A. M. Urbas, T. W. Goo, and Y. L. Kim, "Anderson light localization in biological nanostructures of native silk," *Nat. Commun.* **9**(1), 452 (2018).
29. C. Choi, M. K. Choi, S. Liu, M. S. Kim, O. K. Park, C. Im, J. Kim, X. Qin, G. J. Lee, K. W. Cho, M. Kim, E. Joh, J. Lee, D. Son, S. H. Kwon, N. L. Jeon, Y. M. Song, N. Lu, and D. H. Kim, "Human eye-inspired soft optoelectronic device using high-density MoS<sub>2</sub>-graphene curved image sensor array," *Nat. Commun.* **8**(1), 1664 (2017).
30. J. W. Harris and R. W. Kellermeyer, *The red cell* (Harvard Univ. Press, Cambridge, MA, 1970).
31. H. L. Hsu, W. T. Hsu, and J. Leu, "Effects of environmentally benign solvents in the agarose gel electrolytes on dye-sensitized solar cells," *Electrochim. Acta* **56**(17), 5904–5909 (2011).
32. Q. Xu, F. Liu, Y. X. Liu, W. S. Meng, K. Y. Cui, X. Feng, W. Zhang, and Y. D. Huang, "Aluminum plasmonic nanoparticles enhanced dye sensitized solar cells," *Opt. Express* **22**(S2), A301–A310 (2014).
33. G. Nagaraju, J. H. Lim, S. M. Cha, and J. S. Yu, "Three-dimensional activated porous carbon with meso/macropore structures derived from fallen pine cone flowers: A low-cost counter electrode material in dye-sensitized solar cells," *J. Alloys Compd.* **693**, 1297–1304 (2017).
34. R. L. Konger, Z. Xu, R. P. Sahu, B. M. Rashid, S. R. Mehta, D. R. Mohamed, S. C. DaSilva-Arnold, J. R. Bradish, S. J. Warren, and Y. L. Kim, "Spatiotemporal assessments of dermal hyperemia enable accurate prediction of experimental cutaneous carcinogenesis as well as chemopreventive activity," *Cancer Res.* **73**(1), 150–159 (2013).
35. S. Acikgoz, Y. Ulusu, S. Akin, S. Sonmezoglu, I. Gokce, and M. N. Inci, "Photoinduced electron transfer mechanism between green fluorescent protein molecules and metal oxide nanoparticles," *Ceram. Int.* **40**(2), 2943–2951 (2014).
36. P. H. Wang, Y. X. Tang, Z. L. Dong, Z. Chen, and T. T. Lim, "Ag-AgBr/TiO<sub>2</sub>/RGO nanocomposite for visible-light photocatalytic degradation of penicillin G," *J. Mater. Chem. A Mater. Energy Sustain.* **1**(15), 4718–4727 (2013).
37. A. Khalid, A. N. Mitropoulos, B. Marelli, D. A. Simpson, P. A. Tran, F. G. Omenetto, and S. Tomljenovic-Hanic, "Fluorescent nanodiamond silk fibroin spheres: Advanced nanoscale bioimaging tool," *ACS Biomater. Sci. Eng.* **1**(11), 1104–1113 (2015).
38. S. Nambu, T. Matsui, C. W. Goulding, S. Takahashi, and M. Ikeda-Saito, "A new way to degrade heme: the Mycobacterium tuberculosis enzyme MhuD catalyzes heme degradation without generating CO," *J. Biol. Chem.* **288**(14), 10101–10109 (2013).
39. A. Gorchein, C. K. Lim, and P. Cassey, "Extraction and analysis of colourful eggshell pigments using HPLC and HPLC/electrospray ionization tandem mass spectrometry," *Biomed. Chromatogr.* **23**(6), 602–606 (2009).
40. C. Yuan, H. Z. Li, K. Tang, W. Gärtner, H. Scheer, M. Zhou, and K. H. Zhao, "Near infrared fluorescent biliproteins generated from bacteriophytochrome AphB of *Nostoc* sp. PCC 7120," *Photochem. Photobiol. Sci.* **15**(4), 546–553 (2016).
41. S. Wilaiwan, B. Chirapha, S. Yaowalak, and S. Prasong, "Screening of some elements in different silk cocoon varieties," *J. Appl. Sci. (Faisalabad)* **10**(7), 575–579 (2010).
42. B. Tulachan, S. K. Meena, R. K. Rai, C. Mallick, T. S. Kusurkar, A. K. Teotia, N. K. Sethy, K. Bhargava, S. Bhattacharya, A. Kumar, R. K. Sharma, N. Sinha, S. K. Singh, and M. Das, "Electricity from the silk cocoon membrane," *Sci. Rep.* **4**, 5434 (2014).
43. M. Zurovec, N. Yonemura, B. Kludkiewicz, F. Sehnal, D. Kodrik, L. C. Vieira, L. Kucerova, H. Strnad, P. Konik, and H. Sedadova, "Sericin composition in the silk of *Antheraea yamamai*," *Biomacromolecules* **17**(5), 1776–1787 (2016).
44. X. D. Li, C. T. Gao, H. G. Duan, B. G. Lu, X. J. Pan, and E. Q. Xie, "Nanocrystalline TiO<sub>2</sub> film based photoelectrochemical cell as self-powered UV-photodetector," *Nano Energy* **1**(4), 640–645 (2012).
45. M. Fukuda, K. Kodama, H. Yamamoto, and K. Mito, "Evaluation of new organic pigments as laser-active media for a solid-state dye laser," *Dyes Pigments* **63**(2), 115–125 (2004).
46. J. W. Leem, S. R. Kim, K. H. Choi, and Y. L. Kim, "Plasmonic photocatalyst-like fluorescent proteins for generating reactive oxygen species," *Nano Converg.* **5**(1), 8 (2018).
47. M. I. Asghar, K. Miettunen, J. Halme, P. Vahermaa, M. Toivola, K. Aitola, and P. Lund, "Review of stability for advanced dye solar cells," *Energy Environ. Sci.* **3**(4), 418–426 (2010).